

**Direct measurement of time-frequency analogs of sub-Planck structures**Ludmila Praxmeyer,<sup>1</sup> Chih-Cheng Chen,<sup>1</sup> Popo Yang,<sup>2</sup> Shang-Da Yang,<sup>1</sup> and Ray-Kuang Lee<sup>1,2,3</sup><sup>1</sup>*Institute of Photonics Technologies, National Tsing Hua University, Hsinchu 300, Taiwan*<sup>2</sup>*Department of Physics, National Tsing Hua University, Hsinchu 300, Taiwan*<sup>3</sup>*Physics Division, National Center for Theoretical Science, Hsinchu 300, Taiwan*

(Received 27 May 2015; published 27 May 2016)

Exploiting the correspondence between the Wigner distribution function and the frequency-resolved optical gating (FROG) measurement, we experimentally demonstrate the existence of chessboardlike interference patterns with a time-bandwidth product smaller than that of a transform-limited pulse in the phase-space representation of compass states. Using superpositions of four electric pulses as the realization of compass states, we have shown via direct measurements that displacements leading to orthogonal states can be smaller than limits set by uncertainty relations. In the experiment we observe an exactly chronocyclic correspondence to the sub-Planck structure in the interference pattern appearing for the superposition of two Schrödinger-cat-like states in a position-momentum phase space.

DOI: [10.1103/PhysRevA.93.053835](https://doi.org/10.1103/PhysRevA.93.053835)**I. INTRODUCTION**

It is the superposition principle that leads to interference and diffraction phenomena, determining the evolution of wave packets in classical and quantum systems. When applied to macroscopic objects, the interpretation paradox of the wave function in superposition arises from Schrödinger's gedanken experiment on cat states [1]. By a Schrödinger-cat-like state in quantum optics, one usually understands the coherent superposition of two coherent states, say,  $|\alpha\rangle + |-\alpha\rangle$ . Experimentally, such superpositions were created, e.g., in atomic and molecular systems [2,3], superconducting circuits [4,5], and quantum optical setups [6,7]. It has been noted by Zurek [8] that a superposition of two Schrödinger-cat-like states (four coherent states in total,  $|\alpha\rangle + |-\alpha\rangle + |i\alpha\rangle + | -i\alpha\rangle$ , a so-called *compass state*) in a Wigner phase-space description [9] gives rise to an interference structure that changes rapidly on an area smaller than a Planck's constant  $\hbar$ . The result is counterintuitive because the Heisenberg's uncertainty principle sets a limitation on the simultaneous resolutions in two conjugate observables.

It turns out that the sub-Planck structure determines the scales important to the distinguishability of quantum states [8], and, thereby, potentially has an impact on an ultrasensitive quantum metrology [10,11] and could affect the efficient storage of quantum information [12,13]. In principle, these sub-Planck structures could be used to improve the sensitivity in weak-force detection [14,15] and to help maintain a high fidelity in continuous-variable teleportation protocols [16,17]. In practice, the classical wave optics analogs of sub-Planck structures in the time-frequency domain were observed experimentally so far only for the superposition of two Gaussian pulses [18,19]. Obviously, a single Schrödinger-cat-like state offers a sensitivity to the perturbations only in one direction: perpendicularly to the line joining the coherent states. To provide sensitivity in all directions, another pair of coherent states is needed. Theoretical proposals for the generation of compass states include interactions in cavity-QED systems [13,20], evolution in a Kerr medium [21,22], and fractional revivals of molecular wave packets [23]. Nevertheless, there was no experimental proof in the more complex and demanding

case of the superposition of four pulses. The main technical challenge in the preparation of states separated simultaneously in two conjugate coordinates comes from the difficulty in keeping the coherence among them. Furthermore, performing measurements of such tiny phase-space structures is far from trivial.

In this article, we report a direct measurement of a compass state superposition of four optical pulses and the corresponding interference pattern in the time-frequency domain. The mathematical equivalence between the electric field of an ultrashort pulse and the quantum mechanical wave function of the same shape enables us to observe the phase-space structures through the time-dependent spectrum of light. The experimental data obtained from frequency-resolved optical gating (FROG) measurements of light pulses reveal sub-Planck structure analogs corresponding directly to the compass states. In the interference patterns, areas smaller than those of transform-limited pulses are measured, illustrating that displacements leading to the orthogonality of compass states can be smaller than the Fourier limit imposed on the pulses forming these superpositions.

**II. EXPERIMENTAL SETUP**

As illustrated in Fig. 1(b), in our second-harmonic generation (SHG) FROG measurement [24] the input optical pulse  $E(t)$  is split into two replicas with a tunable time delay by passing through a standard Michelson interferometer. These two mutually delayed replicas mix in a  $\chi^{(2)}$  nonlinear crystal, such as the barium borate (BBO) crystal used in our experiment. Then, a spectrally resolved sum frequency signal is recorded for each time delay  $\tau$ . The resulting time-frequency map (spectrogram) implemented by a nonlinear self-optical gating mechanism can be formulated as the following function for an initial field  $E(t)$ :

$$\mathcal{I}_E^{\text{FROG}}(\tau, \omega) = \left| \int_{-\infty}^{\infty} E(t)E(t - \tau)e^{i\omega t} dt \right|^2. \quad (1)$$

For pulses with real envelopes and a linear phase, the spectrogram (1) is easily mapped to the Wigner quasiprobability

distribution  $W(q, p)$  [9]

$$W(q, p) = \frac{1}{\pi \hbar} \int_{-\infty}^{\infty} e^{2i\xi p/\hbar} F(q - \xi) F^*(q + \xi) d\xi \quad (2)$$

as

$$\mathcal{I}_E^{\text{FROG}}(\tau, \omega) \propto |W(\tau/2, \omega/2)|^2. \quad (3)$$

Here,  $F^*(q)$  denotes the complex conjugate of  $F(q)$ ,  $\hbar$  is set to 1, and our time and frequency domains are represented by  $(\tau, \omega)$ . Moreover, under these conditions, all cross sections of the FROG spectrogram correspond to a scalar product between the probe state  $E(t)$  and its “twin” appropriately shifted in time or frequency [18,25]. Thus, zeros of the cross sections appear for these values of time and frequency shifts that lead to orthogonal states. In the following, we check the scale of the phase-space displacements resulting in distinguishable states based on this property. Let us stress that the data presented here come from direct spectrogram measurements and, unlike typical FROG applications, do not involve steps of state reconstruction.

In our experiment, an Er-doped fiber laser with a 1564 nm center wavelength, 37 nm spectral bandwidth, and 5.68 MHz repetition rate is used as the light source. To construct a compass state, i.e., the superposition of four coherent states, a pulse shaper is introduced to split the input pulse in both time and frequency domains, as illustrated in Fig. 1(a) [26]. Here, a telescope is employed to improve the spectral resolution of the pulse shaper by expanding the beam diameter from 2.8 mm (at the collimator) to 4.5 mm. The input pulse is directly shaped in the frequency domain, through a set of grating, lens, and a spatial light modulator (SLM). The whole spectrum occupies 320 pixels in the SLM, and the throughput of our pulse shaper is around 30%. The spectral separation is realized by blocking the central range of the input spectrum [see Fig. 2(a)], while the temporal separation  $2t_0$  is achieved by imposing an extra

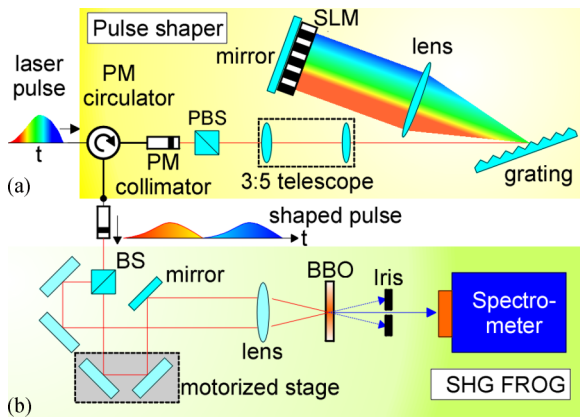


FIG. 1. Schematic view of our experimental setup, where, with the help of a pulse shaper, a superposition of pulses is created and then measured in a SHG FROG setup. The resulting FROG spectrograms are presented in Figs. 3 and 4. Here, (a) a pulse shaper composed of a set of grating, lens, polarization maintain (PM) circulator, polarization maintain (PM) collimator, and spatial light modulator (SLM); (b) SHG FROG composed of a beam splitter (BS) and a motorized stage in one arm to control the time delay  $\tau$ , a nonlinear crystal (BBO) for the second-harmonic generation (SHG), and a spectrometer.

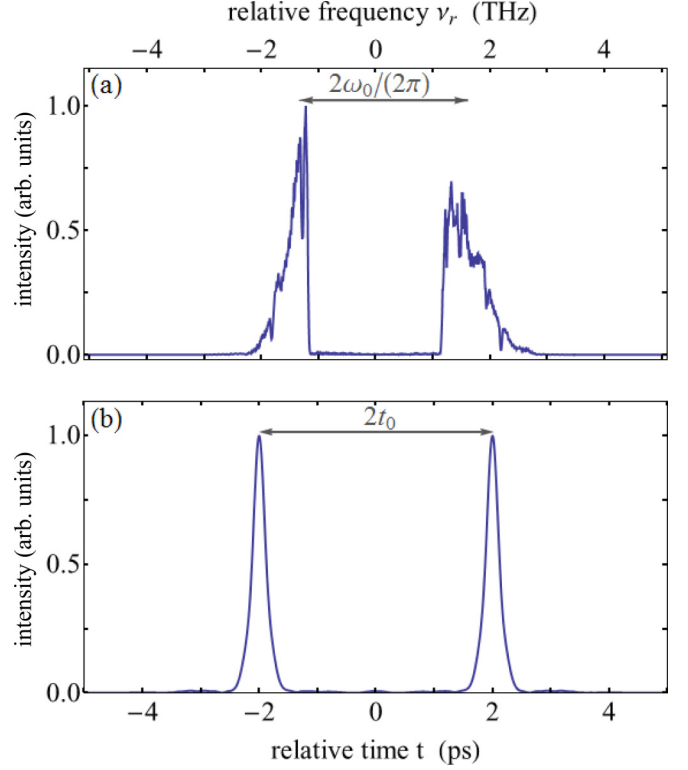


FIG. 2. Typical experimental profiles for our compass states are shown as a function of (a) relative frequency  $\nu_r = \omega/(2\pi)$  and (b) time  $t$ . Here, the four pulses are concurrently separated by  $\omega_0/\pi = 3.3$  THz in frequency and  $2t_0 = 4$  ps in time.

mask function  $M_{\text{SLM}}(\omega) = \cos(\omega t_0) e^{-i\omega t_0}$  via the SLM [27]. The spectrally and temporally separated coherent pulses are further made transform limited by compensating the residual spectral phase via the phase modulation function of the pulse shaper. The power spectrum and temporal intensity of an example are shown in Figs. 2(a) and 2(b), respectively. In total, an initial laser spectra was divided into four pulses separated simultaneously by  $2\omega_0$  in frequency and  $2t_0$  in time, i.e., shaped into our time-frequency representation of the compass state. In our experiments, the spectral resolution is about 0.1 nm, while the delay step size is 6.8 fs. For practical reasons, in the experiment, the separation between pulses in frequency was kept constant while the time separation  $2t_0$  varied from 1.5 to 5 ps.

In the ideal case, when the pulses cut from the initial laser spectrum have Gaussian envelopes, the state generated in a pulse shaper has the form

$$E_{\text{in}}(t) \simeq e^{-(t-t_0)^2 - i(\omega - \omega_0)t} + e^{-(t+t_0)^2 - i(\omega - \omega_0)t} \\ + e^{-(t-t_0)^2 - i(\omega + \omega_0)t} + e^{-(t+t_0)^2 - i(\omega + \omega_0)t}, \quad (4)$$

where  $2t_0$  and  $2\omega_0$  are the time and frequency separations between the Gaussian peaks. For clarity of notation, normalization coefficients and parameters denoting the width of the wave packets are omitted in Eq. (4). Depending on the context, in the following, we will use either a regular frequency  $\nu$  or the corresponding angular frequency  $\omega = 2\pi\nu$ . The compass state  $E_{\text{in}}(t)$  from Eq. (4) is constructed as a superposition of two mutually delayed pairs of pulses with the same carrier

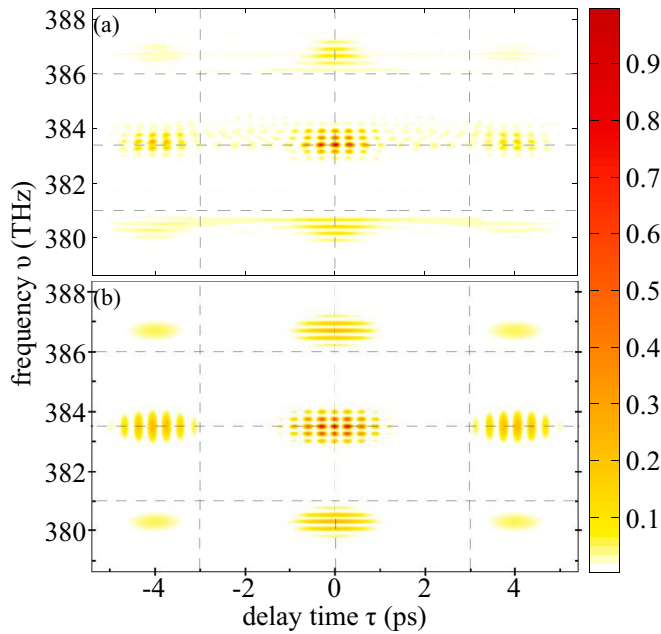


FIG. 3. Compass state in the phase space obtained by (a) a FROG map measured for  $t_0 = 2$  ps, and (b) the numerical simulation calculated for a superposition of four identical Gaussian pulses.

frequency in each pair. The superposition of pulses created in a pulse shaper is then measured in the FROG setup. The resulting spectrograms are presented in Figs. 3 and 4, which correspond

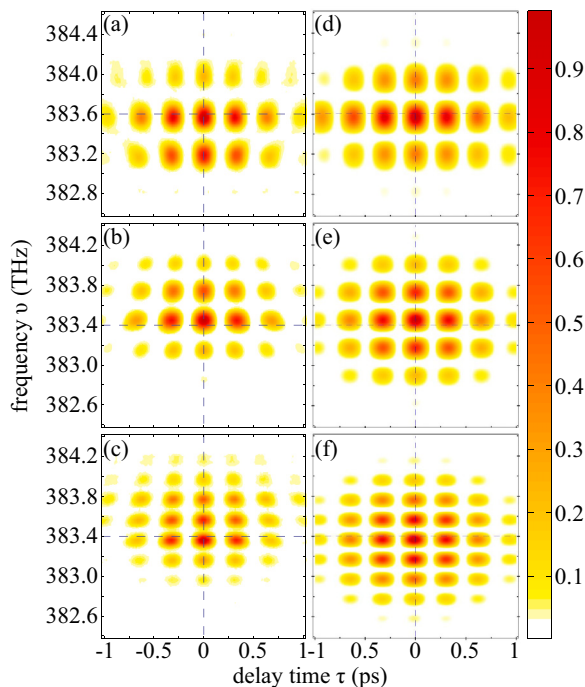


FIG. 4. Zooms of the central interference structure of FROG maps measured for (a)  $t_0 = 1.25$  ps, (b)  $t_0 = 1.75$  ps, and (c)  $t_0 = 2.5$  ps. As a comparison, the corresponding simulations calculated for the compass states built from perfect Gaussian pulses are shown in (d)–(f), respectively.

to the original compass states from the Zurek paper [8] rotated by  $\pi/4$  in the phase space.

### III. THEORETICAL ANALYSIS

A comparison between a theoretical simulation and experimentally obtained time and frequency phase-space maps of compass states is presented in Fig. 3, where spectrograms corresponding to the same time and frequency separation between the cat states are plotted. Experimental data from SHG FROG spectrogram measured for  $t_0 = 2$  ps are shown in Fig. 3(a), while the theoretical plot calculated analytically for perfect Gaussian pulses is presented in Fig. 3(b). In addition to four peaks representing Gaussian wave packets and located at the four corners of the plots, the characteristic patterns of interference fringes are clearly visible between every two of the peaks. Moreover, in the center of four perimeters, a chessboardlike interference pattern appears. In the following, we will verify that for a large enough separation between the peaks this chessboardlike pattern is constructed from areas smaller than  $\Delta\tau\Delta\omega = 1/2$  indicated by the uncertainty relation, which would correspond to sub-Planck areas in the position-momentum phase space. The shape of our pulses is obtained by cutting the laser spectra, and a slight discrepancy between the patterns formed by the real experimental profiles and the theoretically considered ideal Gaussian pulses can be seen between Figs. 3(a) and 3(b).

In the Wigner representation of a compass state, the middle interference pattern is built up from small rectangles of alternating positive and negative values of the function. Even though recordings in the FROG spectrograms take on only non-negative values, areas of the above-mentioned rectangles remain the same, i.e., the distances between subsequent zero lines do not change. For a large enough separation distances between pulses forming the superposition, these areas grow smaller than the area unit defined by the elementary uncertainty relation. In quantum mechanical version, the area unit is equal to  $\hbar/2$ , while in a chronocyclic phase space, it is simply  $1/2$ . It is worth noting that even for smaller separation distances the “sub-Fourier” areas might appear in the FROG maps, namely, areas smaller than those corresponding to dispersion  $\Delta\tau\Delta\omega$  calculated for any of the pulses forming the compass state superposition.

To demonstrate how the interference structure appearing in the middle of the FROG maps changes with a change in the initial parameters, zooms of the central parts of the spectrograms for different time separations between pair of pulses are presented in Fig. 4. Figure 4 shows the zoom of the central interference patterns obtained from the FROG traces for (a)  $t_0 = 1.25$  ps, (b)  $t_0 = 1.75$  ps, and (c)  $t_0 = 2.5$  ps. The corresponding theoretical plots made for superpositions of four identical Gaussian pulses are shown in Figs. 4(d)–4(f), respectively. The comparison serves to illustrate that areas between zero lines of FROG maps indeed decrease with an increasing separation between the pair of pulses. Again, owing to imperfections, the amplitudes of the pulses used in the experiment were not the same and the resulting interference patterns measured are not symmetric with respect to the central wavelength line.

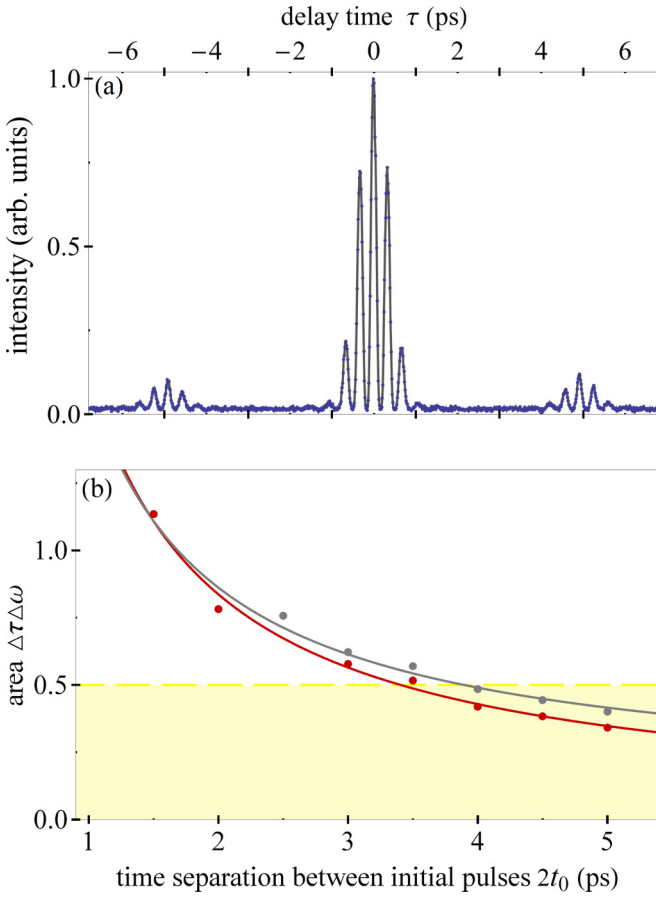


FIG. 5. (a) A central frequency ( $\nu = 383.36$  THz) cross section of the FROG map measured for  $t_0 = 2.5$  ps. Here, blue dots depict the measured intensity values for a given time delay  $\tau$  introduced between two input state copies in the arms of the FROG apparatus. (b) Average areas  $\Delta\tau\Delta\omega$  of the rectangles appearing between the zero lines in the interference structure of the central part of the FROG maps. Values depicted by red or gray dots correspond to two independent sets of experimental data, respectively. The region below the uncertainty relation limit of 0.5 is denoted in yellow.

Finally, let us examine the cross section of the FROG map measured for  $t_0 = 2.5$  ps along the central wavelength  $\lambda = 782$  nm ( $\nu = 383.36$  THz) presented in Fig. 5(a). As mentioned before, the cross sections of the FROG spectrograms give values of the scalar product of a probe field with its ideal copy, but shifted in phase space in a direction perpendicular to the direction defining the cross section. It is clearly seen that the values of the function plotted in Fig. 5(a) decrease to zero between the subsequent peaks. A time shift equal to one half of the distance between the zeros results in superpositions orthogonal to the initial compass state. This result is complementary to the one reported in Ref. [18], where zeros in cross sections defined by  $\tau = 0$  were shown. Figure 5(b) demonstrates how average areas  $\Delta\tau\Delta\omega$  of individual

rectangles forming the central interference pattern change with a change in parameter  $t_0$ . The average values of  $\Delta\tau\Delta\omega$  plotted in Fig. 5(b) are calculated for two independently collected sets of data (depicted by gray or red dots, respectively). These two sets of data are measured for slightly different pulse shapes and differently set time delay resolutions, i.e., different values of the smallest stage-motor step. It is clearly seen that in both cases, for larger separation distances, the areas between zeros indeed reach below the limit imposed by the uncertainty relation. These areas exactly determine a scale of smallest change, ensuring the distinguishability of the mutually shifted states. In principle, there are no limits on how small the interference areas could get. The larger distance is between superposed states, the smaller the size of the chessboard pattern is obtained. However, in practice, the limitation lies in maintaining coherence between superposed states. When they are far apart, maintaining coherence is more difficult and without coherence no interference pattern can be observed. As a last point, we would like to underline that the uncertainty relation is not violated. What we prove here is that a sub-Fourier change of the initial state (shift in frequency and/or time) is enough to produce a state orthogonal to the initial superposition. In the quantum mechanics this leads to a perfect distinguishability of states.

#### IV. CONCLUSION

In summary, using correspondence between FROG maps in a chronocyclic phase space and the Wigner distribution function, we have demonstrated the existence of the interference structure that changes on areas smaller than that of a transform-limited pulse. We have performed FROG measurements of the compass states realized through superpositions of four light pulses constructed with the help of a spatial light modulator (SLM), by manipulating the phase difference in the spectrum. The interpretation of the FROG spectrograms as maps of the values of a scalar product between probe pulses and their shifted copies allowed us to show explicitly that the scale of the changes leading to the orthogonality of states indeed goes below the Fourier limit if sufficient time and frequency separations are simultaneously kept between the input pulses. The sub-Planck structure of the interference pattern in a phase-space representation of the compass states not only manifests itself as a generalized Schrödinger's cat state, but also provides the platform to exploit quantum metrology and quantum information processing through ultrafast optics.

#### ACKNOWLEDGMENTS

This work is supported in part by the Ministry of Science and Technology, Taiwan, under Contracts No. 101-2628-M-007-003-MY4, No. 103-2218-E-007-010, and No. 104-2112-M-007-012-MY3.

[1] E. Schrödinger, Die gegenwärtige Situation in der Quantenmechanik, *Naturwissenschaften* **23**, 807 (1935); **23**, 823 (1935); **23**, 844 (1935).

[2] C. Monroe, D. Meekhof, B. E. King, and D. J. Wineland, A "Schrödinger cat" superposition state of an atom, *Science* **272**, 1131 (1996).

- [3] M. Brune, E. Hagley, J. Dreyer, X. Maître, A. Maali, C. Wunderlich, J. M. Raimond, and S. Haroche, Observing the Progressive Decoherence of the “Meter” in a Quantum Measurement, *Phys. Rev. Lett.* **77**, 4887 (1996).
- [4] J. R. Friedman, V. Patel, W. Chen, S. K. Tolpygo, and J. E. Lukens, Quantum superposition of distinct macroscopic states, *Nature (London)* **406**, 43 (2000).
- [5] C. H. van der Wal, A. C. J. ter Haar, F. K. Wilhelm, R. N. Schouten, C. J. P. M. Harmans, T. P. Orlando, S. Lloyd, and J. E. Mooij, Quantum superposition of macroscopic persistent-current states, *Science* **290**, 773 (2000).
- [6] A. Ourjoumtsev, R. Tualle-Brouri, J. Laurat, and P. Grangier, Generating optical Schrödinger kittens for quantum information processing, *Science* **312**, 83 (2006).
- [7] H. Takahashi, K. Wakui, S. Suzuki, M. Takeoka, K. Hayasaka, A. Furusawa, and M. Sasaki, Generation of Large-Amplitude Coherent-State Superposition via Ancilla-Assisted Photon Subtraction, *Phys. Rev. Lett.* **101**, 233605 (2008).
- [8] W. H. Zurek, Sub-Planck structure in phase space and its relevance for quantum decoherence, *Nature (London)* **412**, 712 (2001).
- [9] E. Wigner, On the Quantum Correction For Thermodynamic Equilibrium, *Phys. Rev.* **40**, 749 (1932).
- [10] D. A. R. Dalvit, R. L. de Matos Filho, and F. Toscano, Quantum metrology at the Heisenberg limit with ion trap motional compass states, *New J. Phys.* **8**, 276 (2006).
- [11] F. Toscano, D. A. R. Dalvit, L. Davidovich, and W. H. Zurek, Sub-Planck phase-space structures and Heisenberg-limited measurements, *Phys. Rev. A* **73**, 023803 (2006).
- [12] J. R. Bhatt, P. K. Panigrahi, and M. Vyas, Entanglement-induced sub-Planck structures, *Phys. Rev. A* **78**, 034101 (2008).
- [13] B. Vlastakis, G. Kirchmair, Z. Leghtas, S. E. Nigg, L. Frunzio, S. M. Girvin, M. Mirrahimi, M. H. Devoret, and R. J. Schoelkopf, Deterministically encoding quantum information using 100-photon Schrödinger cat states, *Science* **342**, 607 (2013).
- [14] U. Roy, S. Ghosh, P. K. Panigrahi, and D. Vitali, Sub-Planck-scale structures in the Pöschl-Teller potential and their sensitivity to perturbations, *Phys. Rev. A* **80**, 052115 (2009).
- [15] J. Dressel, C. J. Broadbent, J. C. Howell, and A. N. Jordan, Experimental Violation of Two-Party Leggett-Garg Inequalities with Semiweak Measurements, *Phys. Rev. Lett.* **106**, 040402 (2011).
- [16] Ph. Jacquod, I. Adagideli, and C. W. J. Beenakker, Decay of the Loschmidt Echo for Quantum States with Sub-Planck-Scale Structures, *Phys. Rev. Lett.* **89**, 154103 (2002).
- [17] A. J. Scott and C. M. Caves, Teleportation fidelity as a probe of sub-Planck phase-space structure, *Ann. Phys.* **323**, 2685 (2008).
- [18] L. Praxmeyer, P. Wasylczyk, Cz. Radzewicz, and K. Wódkiewicz, Time-Frequency Domain Analogues of Phase Space Sub-Planck Structures, *Phys. Rev. Lett.* **98**, 063901 (2007).
- [19] D. R. Austin, T. Witting, A. S. Wyatt, and I. A. Walmsley, Measuring sub-Planck structural analogues in chronocyclic phase space, *Opt. Commun.* **283**, 855 (2010).
- [20] G. S. Agarwal and P. K. Pathak, Mesoscopic superposition of states with sub-Planck structures in phase space, *Phys. Rev. A* **70**, 053813 (2004).
- [21] R. Tanaś, Nonclassical states of light propagating in Kerr media, in *Theory of Nonclassical States of Light*, edited by V. Dodonov and V. I. Mańko (Taylor and Francis, London, 2003).
- [22] M. Stobińska, G. J. Milburn, and K. Wódkiewicz, Wigner function evolution of quantum states in the presence of self-Kerr interaction, *Phys. Rev. A* **78**, 013810 (2008).
- [23] S. Ghosh, A. Chiruvelli, J. Banerji, and P. K. Panigrahi, Mesoscopic superposition and sub-Planck-scale structure in molecular wave packets, *Phys. Rev. A* **73**, 013411 (2006); S. Ghosh, U. Roy, C. Genes, and D. Vitali, Sub-Planck-scale structures in a vibrating molecule in the presence of decoherence, *ibid.* **79**, 052104 (2009).
- [24] R. Trebino, *Frequency-Resolved Optical Gating: The Measurement of Ultrashort Laser Pulses* (Springer, Berlin, 2002).
- [25] J.-C. Diels and W. Rudolph, *Ultrashort Laser Pulse Phenomena*, 2nd ed. (Academic Press, Boston, 2006).
- [26] C.-C. Chen and S.-D. Yang, All-optical self-referencing measurement of vectorial optical arbitrary waveform, *Opt. Express* **22**, 28838 (2014).
- [27] C.-S. Hsu, H.-C. Chiang, H.-P. Chuang, C.-B. Huang, and S.-D. Yang, Forty-photon-per-pulse spectral phase retrieval by modified interferometric field autocorrelation, *Opt. Lett.* **36**, 2611 (2011).